Finite Element Analysis of Slope Stability of Fushun West Open-Pit Mine

Tong WANG*, Lizhi YUAN, Mingli BI

Abstract: Slope stability analysis is the earliest subject that classical soil mechanics tried to solve but has not yet been satisfactorily solved. Various stability analysis methods are roughly equivalent at home and abroad, while the current numerical analysis methods can generally only obtain slope stress, displacement, and plastic zone cannot obtain slope dangerous sliding surfaces and corresponding safety factor. With the development of computer technology, especially the development of nonlinear elastoplastic finite element calculation technology for geotechnical materials, the finite element strength reduction method has attracted attention in recent years. In this paper, the finite element strength reduction method is used to search for the dangerous sliding surface of the slope to obtain the corresponding stability safety factor, and the slope of Fushun West Open-Pit Mine in China is used as an example to analyze the calculation.

Keywords: finite-element method; elastoplastic constitutive model; FE strength reduction method

1 BASIC PRINCIPLE OF FINITE ELEMENT STRENGTH REDUCTION COEFFICIENT METHOD

1.1 Theoretical Background of Finite Element Strength Reduction Method

The finite element method is a method that uses the balance conditions and coordination conditions of the forces on the boundary, constitutive equations, boundary conditions, etc. to analyze the structure. This method can simulate the site conditions more realistically, without assuming the failure surface in advance, and the more realistic failure state can be automatically obtained through analysis [1]. The strength reduction method is to treat the stage without convergence as failure by gradually reducing the shear strength until the calculation no longer converges, and the maximum strength reduction rate of this stage as the minimum safety factor of the slope. This method requires multiple iterations of nonlinear calculation, which is expensive to analyze, and can reduce the calculation time and obtain more accurate results by improving the calculation speed [2].

The advantages of the strength reduction method are as follows [3]: (1) There is no need to assume the failure surface in advance. Failure occurs when the shear strength of soil is less than the shear strength of soil under its own weight. (2) The finite element method does not require the concept of division, and therefore there is no concept of inter-strip force, which satisfies the equilibrium state until the breakdown. (3) If the characteristics of the soil are accurate, the strength reduction coefficient can be obtained by using the information of slope stress and deformation. (4) The strength reduction method can not only understand the deformation process of the failure, but also obtain the information after the failure.

The first paper using the strength reduction method based on the finite element method was a paper published by Zienkiewicz et al. [4]. As shown in Fig. 1, when calculating the safety factor of a slope, we first pay attention to the Gaussian point *A* of any element on the slope, and the stress state of this point is represented by a Mohr's circle. In order to simulate the failure state of a slope, a Mohr's circle of the stress state on the assumed failure surface needs to be close to the failure envelope. Therefore, first assume that the arbitrary safety factor *F* is divided by the shear strength of the point to make it close

to the Mohr circle, that is, the stress state of the point is corrected to the failure state. As the failure point increases, the overall failure of the slope will occur, and the finite element analysis will diverge, and the F value at this time is the minimum safety factor [5].
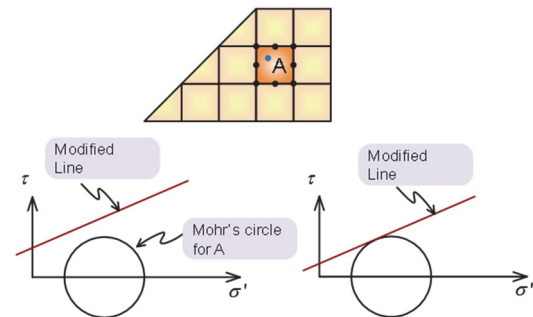

Figure 1 Strength reduction method

1.2 Criterion for Overall Slope Instability

The key question for slope stability analysis using finite element numerical calculations is to determine whether the slope is in an overall failure state according to which criteria [6]. Based on the current judgments of slope failure proposed by scholars at home and abroad, there are the following three points: (1) The prerequisite for overall slope instability is that the plastic zone of the sliding surface or equivalent plastic strain extends from the foot of the slope to the top of the slope [7]. (2) The sudden change in strain and displacement of the slope soil on the sliding surface and the large and unrestricted plastic flow of the soil mass were used as the criterion for the overall instability of the slope [8]. (3) The force or displacement non-convergence calculated by the finite element static equilibrium is used as the criterion for the overall instability of the slope [9].

We judge the overall failure of the slope based on whether the force or displacement obtained by the numerical calculation of the finite element strength reduction method converges or whether the plastic displacement and strain of each node on the sliding surface of the slope rock mass suddenly changes.

The finite element strength reduction method uses the ideal elastoplastic model [10], so the Midas-GTS (SRM) treatment also uses the ideal elastoplastic model.

The mole-Coulomb criterion can be represented in a two-dimensional stress space as follows, as shown in the figure below [11].
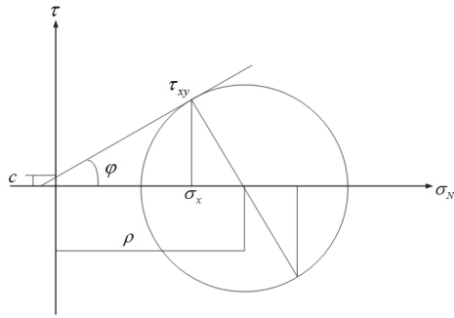

Figure 2 Moore-Coulomb yield conditions for two-dimensional stress spaces

Moore-Coulomb elastoplastic materials only have elastic deformation when they are not yielding, and once they have a yield state, plastic deformation will occur, at which time the plastic deformation will continue to develop until destruction, and the destruction criterion is the yield criterion, so the Moore-Coulomb idea elastoplastic model failure criterion is consistent with the yield criterion [12].

$$\tau = c + \sigma_n \tan\phi \tag{1}$$

where:

$$\sigma_n = \frac{1}{2}(\sigma_x + \sigma_y) - R^{MC}\sin\phi = \frac{1}{2}(\sigma_1 + \sigma_3) - R^{MC}\sin\phi$$

$$R^{MC} = c\cos\phi + \rho\sin\phi = \sqrt{(\sigma_x + \sigma_y)^2/4 + \tau_{xy}^2} = (\sigma_1 + \sigma_3)$$

$$\rho = (\sigma_1 + \sigma_3)/2$$

Because: $\tau = R^{MC}\cos\phi$, obtained: $\sigma_1(1 + \sin\phi) - \sigma_3(1 - \sin\phi) = 2c\cos\phi$.

Bring in the θ_σ, obtained:

$$F = \frac{1}{3}I_1\sin\phi + \left(\cos\phi_\sigma - \frac{1}{\sqrt{3}}\sin\phi_\sigma\sin\phi\right)\sqrt{J_2} - \cos\phi \tag{2}$$

where, $-\dfrac{\pi}{6} \le \theta_\sigma \le \dfrac{\pi}{6}$
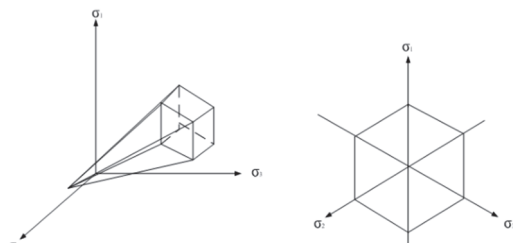

Figure 3 Failure criterion of Mohr-Coulomb ideal elastoplastic model

Mohr-Coulomb The failure criteria for an ideal elastoplastic model are as follows:

$$\frac{\sigma_1 - \sigma_3}{2} = \frac{\sigma_1 + \sigma_3}{2}\sin\phi + \cos\phi \tag{3}$$

where, c - maximum principal stress, Pa, σ_1 - maximum principal stress, Pa, σ_1 - minimum principal stress, Pa, ϕ - the internal friction angle of the technical mass.

1.3 Elasto-Plastic Constitutive Model of Rock and Soil

The establishment of a constitutive model is a key link in numerical simulation. For elastic-plastic geotechnical media, when describing its elastic-plastic constitutive relationship, three sets of equations are generally used, namely the yield condition, the loading-unloading criterion and the basic equation [13] constitutive equation.

(1) The yield conditions and yield surface of the rock.

The initial yield condition is expressed as:

$$f(\sigma_{ij}) = 0 \tag{4}$$

where, f is a function. If plastic deformation occurs, the form of yield conditions changes, which is called subsequent yield conditions, and its expression form becomes:

$$f(\sigma_{ij}, \sigma_{ij}^p, x) = 0 \tag{5}$$

where, σ_{ij} is the total stress, σ_{ij}^p is the plastic stress, and, x is the internal variable of the scalar, which can represent plastic work, plastic volume strain or equivalent plastic strain.

When the yield conditions of elastoplastic geo technical media are analyzed using geometric methods, they can be considered as hypersurfaces in stress space, called yield surfaces [14]. With the emergence and development of plastic strain, according to various factors such as the size and shape of the yield surface, the geotechnical media materials studied are divided into two categories [15]: ideal elastoplastic materials and ideal elastoplastic strengthening materials. With the emergence and development of plastic strain, geotechnical materials in which the size and shape of the yield surface of ideal elastoplastic materials change are called ideal elastoplastic strengthening materials [16]. The stress-strain curves for these two materials are shown below.
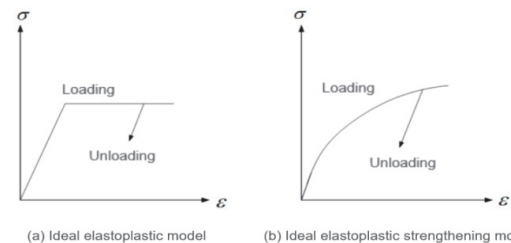

Figure 4 Ideal elastoplastic model and ideal elastoplastic strengthened model

(2) Plastic State Loading-Unloading guidelines.

When the geotechnical medium material is in a plastic state, the reaction to the stress increment exerted on it is generally divided into three types [17]: The first is called plastic loading, which means that after applying the stress increment, the material enters from one plastic state to another, and in this process, new plastic deformation will occur; The second is called neutral load change, which

means that after the stress increment is applied, the state change of the material is similar to the first condition, but in this process, the material does not appear new plastic deformation [18]; The third type is called plastic unloading, which refers to the return of the material from the plastic state to the elastoplastic state after the stress increment is applied, as shown in the following figure.
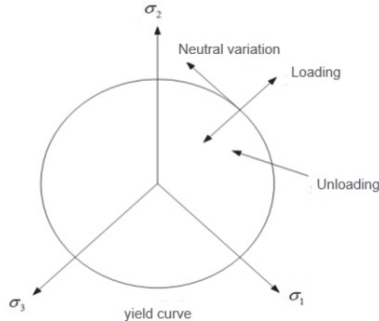

Figure 5 Add-uninstall conditions

Because loading is a process of changing from one plastic state to another, its stress point is always maintained on the yield surface, and when unloading, it is a process of retreating from a plastic state to an elastic state.

(3) Constitutive equations.

When the geotechnical medium material is in a plastic state, the stress-strain relationship of the material is multi-fingered, and its value mainly depends on the properties of the geotechnical medium material itself and the loading-unloading history of the material. If you want to establish the full stress-strain relationship of plastic materials, you can generally only establish the response relationship when the simple loading or plastic deformation is small. For geotechnical media materials, in general, only the relationship between stress and strain increment can be established. When describing the plastic deformation of materials, the theory of the full relationship between stress and strain is called the full theory. The following is a brief introduction to these two theories.

1) Total theory: The full theory was proposed by Wei [19]. In the full theory of plastic mechanics, according to the generalized Hooke's law similar to elastic theory, the following formula was proposed:

$$\sigma_{xx} - \sigma_m = 2G'\left(\varepsilon_{xx} - \varepsilon_m\right),\ \tau_{xy} = G'\gamma_{xy}$$
$$\sigma_{yy} - \sigma_m = 2G'\left(\varepsilon_{yy} - \varepsilon_m\right),\ \tau_{yz} = G'\gamma_{yz}$$
$$\sigma_{zz} - \sigma_m = 2G'\left(\varepsilon_{zz} - \varepsilon_m\right),\ \tau_{zx} = G'\gamma_{zx}$$

Here G' is a parameter related to stress or plastic strain and is a variable, $G' = \sigma_i/3\varepsilon_i$, σ_i is the equivalent force ε_i is an equivalence, ε_m is the volumetric strain, σ_m is the average stress.

2) Increment theory: When the stress produces an infinitesimally small increment, it is assumed that the change of strain can be divided into two parts: elasticity and plasticity: $d\varepsilon_{ij} = d\varepsilon_{ij}^e + d\varepsilon_{ij}^p$.

The elastic stress increment and the elastic strain increment are still connected by the constant elastic matrix D. The plastic strain increment is given by the plastic potential theory. For elastic-plastic media, there is a plastic

potential function Q, which is a function of the stress state and plastic strain, such that: $d\varepsilon_{ij}^p = \lambda \dfrac{\partial Q}{\partial \sigma_{ij}}$

In the formula, λ is a positive undetermined finite quantity, and the specific value is related to the material hardening law. The above formula is called the plastic flow law. For stable ideal elastic-plastic reinforced materials, Q usually takes the same form as the subsequent yield function F. In the special case of $Q = F$, it is called associated plasticity. For associated plasticity, the plastic flow law is expressed as: $d\varepsilon_{ij}^p = \lambda \dfrac{\partial F}{\partial \sigma_{ij}}$.

For the associated plasticity, the total strain increment is expressed as: $d\varepsilon_{ij} = D^{-1}d\sigma_{ij} + \lambda \dfrac{\partial F}{\partial \sigma_{ij}}$.

Depending on the conformance criteria, it can be rolled out: $\lambda = \dfrac{1}{A}\dfrac{\partial F}{\partial \sigma_{ij}}d\sigma_{ij}$.

For ideal elastoplastic materials, there is $A = 0$. When the plastic problem of geotechnical medium materials is solved by incremental theory, although the solution process is more complicated, the theory can accurately describe the plastic deformation law of materials, and at the same time, it can also reflect the influence of strain history on the plastic deformation of materials [20].

1.4 The Method of Calculating the Minimum Safety Factor

When calculating the minimum safety factor, the strength reduction method considers that the elastic modulus E and Poisson's ratio of the slope are unchanged. Gradually reduce the cohesion force c and internal friction angle ϕ as follows until divergence is calculated, taking divergence as the minimum safety factor F_s [21]. at divergence is used as the minimum safety factor.

The formula for the failure safety factor for shear-failed slopes is as follows.

$$F_s = \frac{\tau}{\tau_f} \tag{6}$$

Here τ is the shear strength of the slope, which can be calculated using the More-Coulomb reference as follows.

$$\tau = c + \sigma_n\tan\phi \tag{7}$$

τ_f is the shear stress on the sliding surface and can be calculated as follows:

$$\tau_f = c_f + \sigma_n\tan\phi_f \tag{8}$$

where, $c_f = c/SFR$ and $\phi_f = \tan^{-1}\left(\tan\phi/SFR\right)$ are Shear strength factor; SRF is the Strength reduction factor.

There are two methods for calculating the safety factor of slope strength reserve by finite element value: one is the finite element increment method [22]. The computer is to continuously increase the load, knowing that the safety factor is derived when the damage occurs. The other is the

finite element strength reduction method. Its mechanism is: select the initial reduction coefficient to reduce the soil strength c, ϕ parameters and values, and use finite element software to calculate the reduced parameters until the calculated results do not converge. This reduction coefficient is the reserve safety factor for slope stability, so the corresponding slip surface is the actual sliding surface of the slope [23].

2 MODEL BUILDING
2.1 Of Calculation Parameters

Based on data from slope drilling tests and with reference to relevant specifications and literature [24], the physical and mechanical parameters of the obtained slope are shown in Tab. 1 below.

Table 1 Mechanical parameters of slope rock mass

Material name	Elastic modulus, E / MPa	Poisson's ratio, μ	Cohesion, C / kPa	Angle of friction, ϕ / °	Test weight, γ / kg/m^{-3}
basalt	10000	0.14	120	35	2800
seam	1200	0.29	140	35	1500
oil shale	1700	0.29	200	36	2100
Greenmud stone	1200	0.30	150	30	2300
Clay interlayer	100	0.40	10	9	2300
fault	100	0.40	13	7	1830
Cretaceous sandstone	2000	0.25	58	29	2300
granite gneiss	8000	0.20	150	45	2800

2.2 Selection of Boundary Conditions and Meshing
2.2.1 Meshing

When the physical and mechanical parameters of the rock mass material are constant, the smaller the size of the grid unit, the smaller the time step of the dynamic calculation, which will also lead to greater calculation time and computer memory consumption. Therefore, the size of the grid cells is not as small as possible. At the same time, the size of the grid element is too large and will cause distortion during the wave propagation process, so it is necessary to select a reasonable and correct grid size for the analysis of stability. By monitoring and analyzing models with different mesh sizes, Raman et al. [25] obtained the conclusions in the following table:

Table 2 The relationship between numerical calculation error and grid cell size

Grid cell Dimensions / m	Numerical calculation error			
	P-wave incidence		S-wave incidence	
	positive amplitude	Negative amplitude	positive amplitude	Negative amplitude
30(λ/4)	14.90	24.40	23.51	19.52
20(λ/6)	3.31	3.80	10.48	6.39
15(λ/8)	0.96	0.58	12.20	9.87
12(λ/10)	5.01	3.30	9.95	7.28
10(λ/12)	4.38	0.78	0.39	2.13

When the grid size is 10 m (λ/12), whether it is P wave or S wave incidence, the numerical calculation error is within 5%, which basically eliminates the influence of grid size on numerical calculation accuracy [26]. Therefore, in order to ensure reasonable numerical calculation results, the grid size of the model in this paper is 10 m.

2.2.2 Selection of boundary conditions

The tectonic stress is almost completely released during the stripping of the slope, the process of pit reduction and well mining. Therefore, it is believed that the in-situ stress on the West Open-pit Mine is mainly caused by its own weight, so the model is simplified to a plane stress-strain problem.

The boundary conditions of the finite element model are: the left and right boundaries are constrained horizontally, vertically free, the bottom boundary is constrained in both directions, and the remaining boundaries are free boundaries, as shown in Fig. 6.
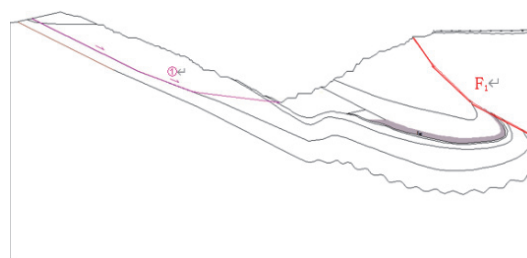

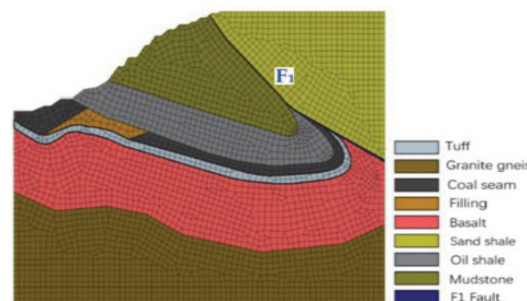**Figure 6** West open-pit slope E400 slope map

Figure 7 Fushun west open-pit mine slope E400 finite element model

In the model, the upper bottom elevation of the slope is +100 m, the lower bottom elevation is –900 m, the slope model length is 1400 m, and the left and right boundary height ranges are 680 m and 1000 m respectively. Since the slope stability analysis mainly focuses on the changes in stress and strength within the rock and soil mass, the slope studied in this paper uses an ideal elastic-plastic model, and the yield criterion of the material is the Moore-Coulomb yield criterion. The slope model established in this article is shown in Fig. 7 below.

2.4 Stability Analysis of of Fushun West Open-Pit Mine
2.4.1 Finite Element Analysis of Slope Static Stability

Through finite element analysis, the total displacement diagram, vertical effective stress diagram and effective plastic strain diagram of the slope are obtained.
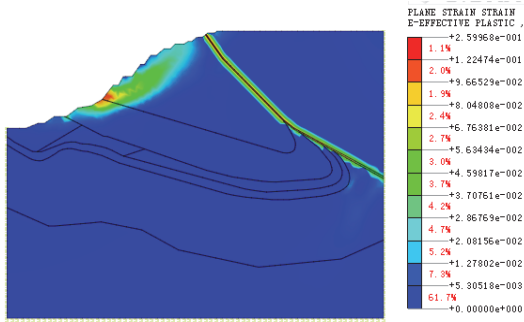
Figure 8 Effective plastic strain diagram of slope

As can be seen from the above figure, the deformation of the place where the fault exists is obvious, and the influence of the fault on the stability of the slope cannot be ignored. Under different reduction coefficient conditions, the effective plastic strain distribution of the slope is shown in Fig. 8 above. As can be seen from the figure, the slope shoulder first appears plastic strain, when the reduction factor F_s = 1.55, the plastic zone basically extends to the top of the slope, forming a sliding surface, at this time the calculation does not converge, so the safety factor of the slope is determined to be 1.55.
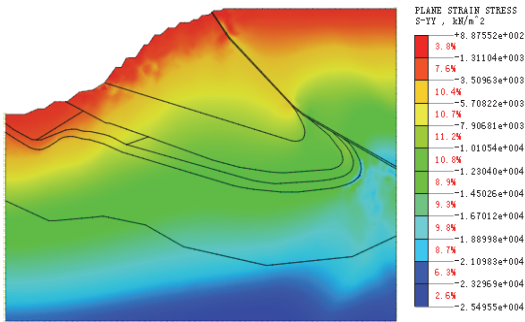

Figure 9 Vertical effective stress

Since most of the middle of the slope is composed of soft rock green mudstone formation, their strength decreases under the action of water and their ability to resist deformation is weakened, and they are more prone to deformation under the action of external force and their own gravity.
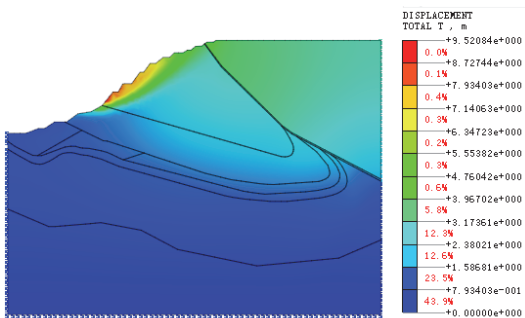

Figure 10 Total slope displacement cloud

The upper disk of the F1 fault has a high density of Cretaceous rock mass and is located above the green mudstone group with low relative density and low stiffness and easy deformation [27]. The creep deformation of the green mudstone group of the soft rock mass itself is large, and the gravity of the Cretaceous rock above the slope makes the slip deformation of the green mudstone group

greater. In turn, the dumping of the upper and lower plates of the F1 fault is more obvious. Sitting slip deformation and toppling deformation dominate the upper part of the slope and the surface deformation, and the deformation is large and significant.

2.4.2 Distribution and Regular Characteristics of Deformation and Damage Zones

The deformation of the reverse dip rock layer produces deformation cracks in the upper disk of the F1 fault, causing the relaxation of the Cretaceous rock mass to follow and deform, and multiple tensile cracks and surface subsidence on the surface, here is the relaxation deformation zone. The reverse dipping rock layer transmits the dumping force downward and squeezes the lower soft rock mass. The green mudstone formation glides along the intersection with the oil shale, where the slip deformation is the first to occur.
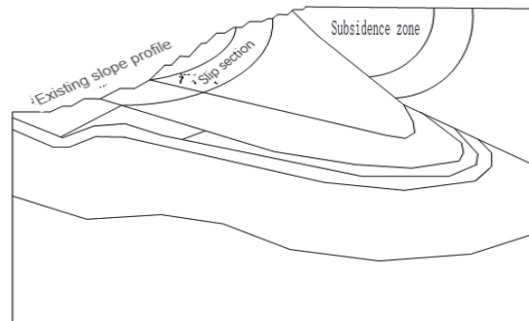

Figure 11 Schematic diagram of failure mode of subsidence and slippage

Bedding slip zone is located in the green mud and brown shale inter beddite group at the top of the slope, due to the existence of weak layers of brown shale, the deformation is mainly along the slip, the amount of slip gradually decreases with the increase of burial depth, and the closer to the top of the slope, the greater the amount of slippage. Dumping and subsidence areas in the Cretaceous and Fourth Combined Rock Formations located north of the F1 fault, the deformation in this area is mainly dumping deformation and subsidence failure, that is, it is initially dumped deformation and then developed into subsidence failure. Located in the slip zone Located on the north side of the F1 fault. The upright inverted rock formation on the north slope and the dumping deformation of the F1 fault zone caused the rock mass on the north side of the F1 fault to be suspended and lost support, resulting in sit-slip. Weak deformation zone refers to the part outside the above-mentioned deformation and destruction zone.

3 CONCLUSIONS

This paper first introduces the finite element strength reduction method, and briefly explains its advantages and practicality. On this basis, a static stability analysis was conducted on the slope of Fushun West Open-pit Mine in China, which is the object of analysis in this article. The dangerous sliding surface of the slope was searched and the corresponding stability safety factor was 1.5. In addition, the deformation mechanism under static force of Fushun West open-pit mine edge was analyzed and studied. The slope of Fushun West open-pit mine is composed of coal

strata. The coal seam is brittle and easy to disintegrate, the compressive and shear resistance is weak. This set of strata under the condition of having an empty surface, even if there is no other factor of influence, will also make the rock mass slide in the direction of the air under the combined force of the rock mass from gravity and horizontal in-situ stress. Sliding surfaces tend to consist of fractured surfaces or layers with an angle greater than the angle of the slope surface.

4 REFERENCES

[1] Ojo, O. & Shittu, R. (2023). Design and finite element method based structural analysis of a pet bottles-to-plastic flakes recycling plant. *International Journal of Industrial Engineering and Management, 14*(1), 25-40. https://doi.org/10.24867/IJIEM-2023-1-322

[2] Li, H. L., Zhang, Z. Q., & Yang, W. (2021). Stability analysis of slope based on limit equilibrium method and strength reduction method. *Annales de Chimie Science des Matériaux, 45*(5), 379-384. https://doi.org/10.18280/acsm.450503

[3] Zhao, L., Sun, X., Liu, F., Wang, P., & Chang, L. (2022). Study on morphological identification of tight oil reservoir residual oil after water flooding in secondary oil layers based on convolution neural network. *Energies, 15*(15), 5367. https://doi.org/10.3390/en15155367

[4] Zienkiewicz, O. C., Humpheson, C., & Lewis, R. W. (1975). Associated and non-associated visco-plasticity and plasticity in soil mechanics. *Geotechnique, 25*(4), 671-689. https://doi.org/10.1680/geot.1975.25.4.671

[5] Yang, Z., Guo, N., & Zhang, H. (2021). Study on microstructure characteristics of clay rock of Xigeda formation in Xichang city based on softening test and image recognition. *In Hydraulic and Civil Engineering Technology VI*, 73-78. https://doi.org/10.3233/ATDE210151

[6] Mahmood, N. S., Aude, S. A., Abdullah, H. H., Sulaiman, S. O., & Al Ansari, N. (2022). Analysis of slope stability and soil liquefaction of zoned earth dams using numerical modeling. *International Journal of Design & Nature and Ecodynamics, 17*(4), 557-562. https://doi.org/10.18280/ijdne.170409

[7] Li, X., Su, D., Chang, D., Liu, J., Wang, L., Tian, Z., Wang, S. X., & Sun, W. (2023). Multi-scale feature extraction and fusion net: Research on UAVs image semantic segmentation technology. *Journal of ICT Standardization, 11*(1), 97-116. https://doi.org/10.13052/jicts2245-800X.1115

[8] Zou, P., Teng, Y., & Niu, T. (2022). Multi-scale feature extraction and fusion for online knowledge distillation. *International Conference on Artificial Neural Networks*, Bristol, UK, 126-138. https://doi.org/10.1007/978-3-031-15937-4

[9] Hu, W., Wang, T., Wang, Y., Chen, Z., & Huang, G. (2022). LE–MSFE–DDNet: A defect detection network based on low-light enhancement and multi-scale feature extraction. *The Visual Computer, 38*(11), 3731-3745. https://doi.org/10.1007/s00371-021-02210-6

[10] Jeon, B. U. & Chung, K. (2022). CutPaste-based anomaly detection model using multi scale feature extraction in time series streaming data. *KSII Transactions on Internet & Information Systems, 16*(8), 2787-2800. https://doi.org/10.3837/tiis.2022.08.018

[11] Micó, V. & García, J. (2010). Common-path phase-shifting lensless holographic microscopy. *Optics Letters, 35*(23), 3919-3921. https://doi.org/10.1364/OL.35.003919

[12] Raman, N., Shah, S., & Veloso, M. (2022). Synthetic document generator for annotation-free layout recognition. *Pattern Recognition, 128*, 108660. https://doi.org/10.1016/j.patcog.2022.108660

[13] Chai, S., Zhuang, L., & Yan, F. (2023). LayoutDM: Transformer-based diffusion model for layout generation. *Proceedings of the IEEE/CVF Conference on Computer Vision and Pattern Recognition*, 18349-18358. https://doi.org/10.1109/CVPR52729.2023.01760

[14] Tan, Z., Chu, Q., Chai, M., Dongdong, C., Jing, L., & Qiankun, L. (2022). Semantic probability distribution modeling for diverse semantic image synthesis. *IEEE Transactions on Pattern Analysis and Machine Intelligence, 45*(5), 6247-6264. https://doi.org/10.1109/TPAMI.2022.3210085

[15] Liu, J., Du, W., Zhou, C., & Qin, Z. (2021). Rock Image Intelligent Classification and Recognition Based on Resnet-50 Model. *Journal of Physics: Conference Series, 2076*(1), 012011. https://doi.org/10.1088/1742-6596/2076/1/012011

[16] Zhao, L., Sun, X., Liu, F., Wang, P., & Chang, L. (2022). Study on morphological identification of tight oil reservoir residual oil after water flooding in secondary oil layers based on convolution neural network. *Energies, 15*(15), 5367. https://doi.org/10.3390/en15155367

[17] Lai, J., Liu, B. C., Li, H. B., Pang, X. J., Liu, S. C., Bao, M., & Wang, G. W. (2022). Bedding parallel fractures in fine-grained sedimentary rocks: recognition, formation mechanisms, and prediction using well log. *Petroleum Science, 19*(2), 554-569. https://doi.org/10.1016/j.petsci.2021.10.017

[18] Yang, Z., Guo, N., & Zhang, H. (2021). Study on microstructure characteristics of clay rock of Xigeda formation in Xichang city based on softening test and image recognition. *Hydraulic and Civil Engineering Technology VI*, 73-78. https://doi.org/10.3233/ATDE210151

[19] Wei, W., Li, L., Shi, W.F., & Liu, J.P. (2021). Ultrasonic imaging recognition of coal-rock interface based on the improved variational mode decomposition. *Measurement*, 170, 108728. https://doi.org/10.1016/j.measurement.2020.108728

[20] Li, X., Su, D., Chang, D., Liu, J., Wang, L., Tian, Z., Wang, S. X., & Sun, W. (2023). Multi-scale feature extraction and fusion net: Research on UAVs image semantic segmentation technology. *Journal of ICT Standardization, 11*(1), 97-116. https://doi.org/10.13052/jicts2245-800X.1115

[21] Zou, P., Teng, Y., & Niu, T. (2022). Multi-scale feature extraction and fusion for online knowledge distillation. *International Conference on Artificial Neural Networks*, Bristol, UK, 126-138. https://doi.org/10.1007/978-3-031-15937-4

[22] Hu, W., Wang, T., Wang, Y., Chen, Z., & Huang, G. (2022). LE–MSFE–DDNet: A defect detection network based on low-light enhancement and multi-scale feature extraction. *The Visual Computer, 38*(11), 3731-3745. https://doi.org/10.1007/s00371-021-02210-6

[23] Jeon, B. U. & Chung, K. (2022). CutPaste-based anomaly detection model using multi scale feature extraction in time series streaming data. *KSII Transactions on Internet & Information Systems, 16*(8), 2787-2800. https://doi.org/10.3837/tiis.2022.08.018

[24] Micó, V. & García, J. (2010). Common-path phase-shifting lensless holographic microscopy. *Optics Letters, 35*(23), 3919-3921. https://doi.org/10.1364/OL.35.003919

[25] Raman, N., Shah, S., & Veloso, M. (2022). Synthetic document generator for annotation-free layout recognition. *Pattern Recognition, 128*, 108660. https://doi.org/10.1016/j.patcog.2022.108660

[26] Chai, S., Zhuang, L., & Yan, F. (2023). LayoutDM: Transformer-based diffusion model for layout generation. *Proceedings of the IEEE/CVF Conference on Computer Vision and Pattern Recognition*, 18349-18358. https://doi.org/10.1109/CVPR52729.2023.01760

Contact information:

Tong WANG, PhD, Lecture
(Corresponding author)
School of Prospecting & Surveying Engineering,
Changchun Institute of Technology,
Changchun, China 130061
E-mail: wangtong@ccit.edu.cn

Lizhi YUAN, Senior Engineer
Jilin Province Water Conservancy And Hydroelectric Engineering Bureau
Grovpco, Co. Ltd,
Changchun, China 130061
E-mail: yuanlizhi2008@sohu.com

Mingli BI, PhD, Lecture
School of Prospecting & Surveying Engineering,
Changchun Institute of Technology,
Changchun, China 130061
E-mail: 0215049@ccit.edu.cn